

RESEARCH ARTICLE

First-Principles Calculations, Experimental Study, and Thermodynamic Modeling of the Al-Co-Cr System

Xuan L. Liu^{1*}, Thomas Gheno², Bonnie B. Lindahl³, Greta Lindwall¹, Brian Gleeson², Zi-Kui Liu¹

1 Department of Materials Science and Engineering, The Pennsylvania State University, University Park, Pennsylvania, 16802, United States of America, **2** Department of Mechanical Engineering and Materials Science, University of Pittsburgh, Pittsburgh, Pennsylvania, 15261, United States of America, **3** Department of Materials Science and Engineering, KTH Royal Institute of Technology, SE-100 44, Stockholm, Sweden

* xul119@psu.edu



OPEN ACCESS

Citation: Liu XL, Gheno T, Lindahl BB, Lindwall G, Gleeson B, Liu Z-K (2015) First-Principles Calculations, Experimental Study, and Thermodynamic Modeling of the Al-Co-Cr System. *PLoS ONE* 10(4): e0121386. doi:10.1371/journal.pone.0121386

Academic Editor: Dennis Salahub, University of Calgary, CANADA

Received: December 3, 2014

Accepted: January 31, 2015

Published: April 13, 2015

Copyright: © 2015 Liu et al. This is an open access article distributed under the terms of the [Creative Commons Attribution License](https://creativecommons.org/licenses/by/4.0/), which permits unrestricted use, distribution, and reproduction in any medium, provided the original author and source are credited.

Data Availability Statement: All relevant data are within the paper and its Supporting Information files.

Funding: XLL, GL, and ZKL acknowledges that the computational aspects of this work were financially supported by the NSF Industry/University Cooperative Research Center for Computational Materials Design (CCMD, <http://www.ccmd.psu.edu/>), including dues contributions of CCMD members, through grants IIP-1034965 (Penn State) and IIP-1034968 (Georgia Tech) and the Office of Naval Research (ONR, <http://www.onr.navy.mil/>) with the contract number N0014-07-1-0638 managed by

Abstract

The phase relations and thermodynamic properties of the condensed Al-Co-Cr ternary alloy system are investigated using first-principles calculations based on density functional theory (DFT) and phase-equilibria experiments that led to X-ray diffraction (XRD) and electron probe micro-analysis (EPMA) measurements. A thermodynamic description is developed by means of the calculations of phase diagrams (CALPHAD) method using experimental and computational data from the present work and the literature. Emphasis is placed on modeling the bcc-A2, B2, fcc- γ , and tetragonal- σ phases in the temperature range of 1173 to 1623 K. Liquid, bcc-A2 and fcc- γ phases are modeled using substitutional solution descriptions. First-principles special quasirandom structures (SQS) calculations predict a large bcc-A2 (disordered)/B2 (ordered) miscibility gap, in agreement with experiments. A partitioning model is then used for the A2/B2 phase to effectively describe the order-disorder transitions. The critically assessed thermodynamic description describes all phase equilibria data well. A2/B2 transitions are also shown to agree well with previous experimental findings.

Introduction

Nickel-base superalloys used in the hot sections of gas turbines require corrosion-resistant coatings to withstand the harsh thermo-chemical conditions prevailing in these combustion environments [1,2]. Overlay MCrAlY (M = Ni, Co or NiCo) coatings are widely used for this purpose, either solely or in conjunction with a thermally insulating ceramic topcoat, most commonly yttria-stabilized zirconia, to comprise a thermal barrier coating (TBC) system [3–6]. During service, microstructural evolution of the MCrAlY layer arises as a result of temperature variations, reactions with the environment such as selective oxidation removing Al from the subsurface, or interdiffusion with the substrate material, driven by differences in chemical

David Shiffer. TG and BG acknowledges that the experimental aspects of this work were partly supported by the Department of Energy under grant number DE-FE0007271 through the University Turbine Systems Research (UTSR) Program run by the National Energy Technology Laboratory (NETL, <http://www.netl.doe.gov/>), with Dr. Seth Lawson being the Project Manager. One of the authors, BL, acknowledges funding from the European Research Fund for Coal and Steel (RFCS, <http://cordis.europa.eu/coal-steel-rtd/>) project "Precipitation in High Manganese Steels" under the grant agreement no. RFSR-CT-2010-00018. The funders had no role in study design, data collection and analysis, decision to publish, or preparation of the manuscript.

Competing Interests: The authors have declared that no competing interests exist.

potentials. A good knowledge of the alloy thermodynamics is critical to understanding and predicting these evolutionary processes, which in turn affect the corrosion resistance and mechanical properties of the system.

Computational design of effective MCrAl-based coating compositions necessitates a thermodynamic description methodology which can predict phase compositions and fractions at the temperatures of interest. One such method is CALPHAD, which has been used extensively and successfully in the thermodynamic modeling of many multi-component systems including Ni-base superalloys [7,8]. The CALPHAD approach parameterizes the Gibbs energy functions of all phases in unary, binary and ternary systems using computational and experimental data on phase equilibria and thermochemistry. The parameters are entered in a database and extrapolations to multi-component systems can be made. Limitations are known to exist in the current description of the quaternary Al-Co-Cr-Ni system for Co contents in excess of 20 wt. % [9,10] which are common in practice [2,11,12]. While assessment of the Al-Cr-Ni system has been well documented [7], the thermodynamic properties of the Al-Co-Cr system have not been adequately assessed.

Phases important to coating systems are B2 (β , $Pm\bar{3}m$, simple cubic type) and fcc-A1 (γ , $Fm\bar{3}m$, disordered f.c.c.). However, bcc-A2 (α , $Im\bar{3}m$, disordered b.c.c.), hcp-A3 (ϵ , $P6_3/mmc$, disordered h.c.p.) and sigma (σ , $P4_2/mnm$, Frank-Kasper) must also be modeled to allow for a complete description. One important feature of the Al-Co-Cr system is the A2/B2 second-order transformation at temperatures above 1373 K [13]. The present study aims to construct a thermodynamic model accounting for the A2/B2 ordering phenomenon, where atoms take on distinct lattice sites in B2. The two phases have vastly different compositions at low temperatures, but merge to similar compositions at higher temperatures which has to be accounted for in the thermodynamic model.

As phase equilibrium data are scarce, especially in the important B2+ γ + σ region, experiments are conducted in this study at 1173, 1273, and 1373 K to aid the thermodynamic modeling. Additionally, first-principles calculations based on density functional (DFT) theory are incorporated to supplement the lack of experimentally measured thermochemical data in the ternary system [14] as well as to study the A2+B2 miscibility gap that is prevalent over the entire phase diagram. Ultimately, this system will be used in the construction of a multicomponent Al-Co-Cr-Ni-Y database. As a result, this database needs to be compatible with previously modeled Al-Co-Ni [15] and Al-Cr-Ni [7] systems.

The Al-Co thermodynamic model assessed by Dupin and Ansara [16] is adopted in the present work. This will allow compatibility with Dupin's [15] model of the Al-Co-Ni system. The Co-Cr system modeled by Oikawa et al. [17] is found to successfully capture experimental activity [18], enthalpy [18] and phase boundary data [17], which are crucial toward the extension to the Al-Co-Cr ternary, and is therefore adopted here. It also allows compatibility with the modeling of the Co-Cr-Ni system by Yang et al. [19], which would enable modeling of the quaternary Al-Co-Cr-Ni system. In Oikawa et al.'s [17] treatment of the Co-Cr system, no indication of B2 ordering was reported, hence the B2 phase will be modeled as a metastable phase with data from first-principles calculations. Saunders' [20] assessment of the Al-Cr system, used in COST507, is used here. Its description of the composition range of some intermetallics is not complete, but this will be shown to have no impact on the Al-Co-Cr system at the temperatures of interest in this study. Although XRD data from Helander and Tolochko [21] indicate a possible B2 ordering, no A2 to B2 second-order transition has been conclusively established in the Al-Cr system. Following Dupin et al. [7] who noted that a A2/B2 transition would modify the A2-AlCr₂ phase boundary and require additional experimental data for proper assessment, the B2-AlCr phase is not included here.

Ishikawa et al. [13] investigated the Al-Co-Cr system in the temperature range 1273–1623 K using multi-phase alloys and diffusion couples. Isotherms at 1573 and 1623 K showed complete dissolution of σ and a particularly large composition range for the B2 phase. The experimental work also provided compositions for the A2/B2 order-disorder transition at 1473 K and above, which are important to the present modeling. Previous models are combined with ternary data from the literature and this work to produce the overall thermodynamic description.

Materials and Methods

Experimental procedures

Ingots of nominal compositions (at. %) Co-20Cr-20Al-0.4Y (# A4), Co-26Cr-11Al-0.1Y (A5), Co-35Cr-6Al-0.1Y (A6) and Co-35Cr-11Al-0.1Y (A7) were prepared by arc-melting and drop-cast in a chamber evacuated and back-filled with 0.5 atm of argon. Specimens were cut to approximate dimensions of 10 x 10 x 1 mm, vacuum-encapsulated in quartz capsules, homogenized for 48 h at 1423 K in a tube furnace, and slowly brought to equilibration temperature. Equilibration treatments were conducted at 1173, 1273 and 1373 K for 500, 200 and 100 h, respectively, followed by water quenching to retain the equilibrated microstructures. Phase constitutions were studied by X-ray diffraction (XRD) with a PANalytical Empyrean instrument, using a Co radiation source ($K_{\alpha 1} = 1.789 \text{ \AA}$).

Polished sections of the heat-treated alloys were prepared by standard metallographic procedures. Phase compositions were determined by electron probe micro-analysis (EPMA) using a JEOL JXA-8530F field emission gun instrument. For each element, measured intensities were converted to concentrations by interpolation via a calibration curve built using a series of standards of known compositions (chemical analysis by inductively coupled plasma mass spectrometry). The probe size used during measurements was about 1 μm , and the alloy microstructures were sufficiently coarse for each phase to be analyzed individually.

CALPHAD thermodynamic models

Solution phases: bcc, fcc (γ), hcp (ϵ), and liquid. In the present work, the Gibbs energies of γ , ϵ , and liquid solution phases are modeled using the following equation based on a single sublattice,

$$G_m^\Phi = \sum x_i {}^\circ G_i^\Phi + RT \sum x_i \ln x_i + {}^{XS} G_m^\Phi + RT {}^{Magnetic} G_m^\Phi \quad \text{Eq.1}$$

where ${}^\circ G_i^\Phi$ represents the molar Gibbs energy of the pure elements, $i = \text{Al, Co, Cr}$, with structure Φ taken from the SGTE Unary PURE4 database [22], and the other symbols have their usual meanings. In Eq. 1, the first term represents the physical mixing of the elements and the second term is the contribution from the ideal entropy of mixing. The excess term, ${}^{XS} G_m^\Phi$, is modeled using a Redlich-Kister polynomial [23] to represent the non-ideal interactions between Al, Co and Cr, as shown below:

$$\begin{aligned} {}^{XS} G_m^\Phi = & \sum_i \sum_{j>i} x_i x_j \sum_{v=0}^v L_{i,j}^\Phi (x_i - x_j) \\ & + \sum_i \sum_{j>i} \sum_{k>j} x_i x_j x_k [{}^1 L_{i,j,k}^\Phi (x_i + \delta_{i,j,k}) + {}^2 L_{i,j,k}^\Phi (x_j + \delta_{i,j,k}) + {}^3 L_{i,j,k}^\Phi (x_k + \delta_{i,j,k})] \end{aligned} \quad \text{Eq.2}$$

Where $\delta_{i,j,k} = (1 - x_i - x_j - x_k) / 3$. The binary and ternary interaction terms, ${}^v L_{i,j}^\Phi$ and ${}^v L_{i,j,k}^\Phi$, are expressed in the form $A + B \times T$ where A and B are the model parameters to be evaluated. Due to the ferromagnetic nature of Co and the antiferromagnetic nature of Cr, ${}^{Magnetic} G_m^\Phi$ is included to capture magnetic contributions to the Gibbs energy [24,25]. Hillert and Jarl [24] expressed the

magnetic contribution as:

$$G_m^{\text{Magnetic}} = RT \ln(\beta + 1) f(\tau) \tag{Eq.3}$$

where β represents the average magnetic moment and the function $f(\tau)$ is related to the Curie temperature (T_C):

$$f(\tau) = 1 - \frac{1}{A} \left[\frac{79\tau^{-1}}{140p} + \frac{474}{497} \left(\frac{1}{p} - 1 \right) \left(\frac{\tau^3}{6} + \frac{\tau^9}{135} + \frac{\tau^{15}}{600} \right) \right], \text{ if } \tau = \frac{T}{T_C} \leq 1$$

$$f(\tau) = -\frac{1}{A} \left(\frac{\tau^{-5}}{10} + \frac{\tau^{-15}}{315} + \frac{\tau^{-25}}{1500} \right), \text{ if } \tau = \frac{T}{T_C} \geq 1 \tag{Eq.4}$$

$$A = \frac{518}{1125} + \frac{11,692}{15,975} \left(\frac{1}{p} - 1 \right)$$

The constant p takes on values of 0.28 for fcc and hcp metals and 0.4 for bcc metals.

To account for the A2/B2 order-disorder transition, the bcc phase is modeled using the partitioning model, which treats the ordered and disordered components separately [26]. The disordered component of A2 is described using Eq. 1, and the model for the ordered component is described in the next section. Additionally, triple-defect mechanisms are especially important when considering site ordering in B2-aluminide-containing systems such as Al-Co [16], Al-Fe [27] or Al-Ni [7]. To account for this phenomenon [29] when the A2 phase is combined with the B2 phase, vacancies have been introduced in the substitutional sublattice of the A2 phase model as in Ref. [26]. Ordering of the bcc phase will be described in the following section.

Intermetallic phases: B2 and σ

The two ordered phases, B2 and σ , are described using sublattice models based on the compound energy formalism (CEF) [28]. In order to describe the A2/B2 ordering for the bcc phase, both A2 and B2 are modeled using a single Gibbs energy function where the ordered part (B2) is described by a sublattice formula $(\text{Al,Co,Cr,Va})_1(\text{Al,Co,Cr,Va})_1$ and the disordered part (A2) by $(\text{Al,Co,Cr,Va})_1$. Specifically, B2 is appended to the already existing A2 model. Then, as implemented in Thermo-Calc, free energy minimization determines whether A2 and/or B2 are stable depending on the input conditions. In addition, a set of parameterization constraints derived by Dupin and Ansara [26] are used to partition the ordered and disordered parts of the A2/B2 Gibbs energy to allow independent evaluations. The B2 phase contains six stoichiometric compounds, or "end-members" (excluding vacancies) which represent the reference states generated when pure components fully occupy a sublattice; i.e. B2-(Al)(Al), B2-(Al)(Co), B2-(Al)(Cr), B2-(Co)(Cr), B2-(Co)(Co), and B2-(Cr)(Cr). The end-members of the B2 phase in the present system all come from binary systems and as a result, their formation energies are fixed by the previous Al-Co and Al-Cr binary assessments in this model; B2 is not included in the Co-Cr assessment by Oikawa et al. [17] and is therefore modeled in the present work.

The partitioning model describes the A2 and B2 with one single Gibbs energy function and the same sublattice model, $(\text{Al,Co,Cr,Va})_1(\text{Al,Co,Cr,Va})_1$. As a result, the Gibbs energy of A2 combined with B2 is described as:

$$G_m^{\alpha/\beta} = G_m^\beta(x_i) + \Delta G_m^{\text{order}}(y_i^{(s)}) \tag{Eq.5}$$

to include contributions from the disordered solution, $G_m^\beta(x_i)$, in A2 as well as from the ordered B2 itself, $\Delta G_m^{\text{order}}(y_i^{(s)})$. Here, $\Delta G_m^{\text{order}}(y_i^{(s)})$ can be separated into two terms, and the total Gibbs

energy of A2 and B2 becomes:

$$G_m^{\alpha/\beta} = G_m^\alpha(x_i) + G_m^{\beta(O)}(y_i^{(s)}) - G_m^{\beta(O)}(y_i^{(s)} = x_i) \tag{Eq.6}$$

where $y_i^{(s)}$ denotes the site fraction of element i on sublattice s . It can be seen that the ordering independent term, $G_m^\alpha(x_i)$, and the ordering dependent terms $G_m^{\beta(O)}(y_i^{(s)})$ and $G_m^{\beta(O)}(y_i^{(s)} = x_i)$ are separated in a way to allow each to be modeled independently. The term $G_m^{\beta(O)}(y_i^{(s)})$ takes on the partitioned form, as described by Dupin and Ansara [26]:

$$\begin{aligned} G_m^{\beta(O)}(y_i^{(s)}) &= \sum_i \sum_j (y_i' y_j'' \circ G_{ij}^{\beta(O)} + y_j' y_i'' \circ G_{ji}^{\beta(O)}) + RT[\sum_i y_i' \ln(y_i') + \sum_j y_j'' \ln(y_j'')] \\ &+ \sum_i \sum_j \sum_k \{y_i' y_j' y_k'' [\sum_k v L_{i,j,k}^{\beta(O)} (y_i' - y_j')^v]\} + \sum_i \sum_j \sum_k \{y_k' y_i'' y_j'' [\sum_k v L_{k,i,j}^{\beta(O)} (y_i'' - y_j'')^v]\} \\ &+ \sum_i \sum_j \sum_k \sum_l y_i' y_j' y_k'' y_l'' v L_{i,j,k,l}^{\beta(O)} + \sum_i \sum_j \sum_k \sum_l (y_i' y_j' y_k'' y_l'' v L_{i,j,k,l}^{\beta(O)} + y_i'' y_j'' y_k' y_l' v L_{l,i,j,k}^{\beta(O)}) \end{aligned} \tag{Eq.7}$$

When the phase becomes disordered, i.e. $y_i' = y_i'' = x_i$, $G_m^{\beta(O)}(y_i^{(s)}) - G_m^{\beta(O)}(y_i^{(s)} = x_i)$ equals zero and eliminates the ordering energy contribution. The equivalence of the CEF and partitioned models is obtained using $2G_m^{Partition}(y_i^{(s)}) = G_m^{CEF}(y_i^{(s)})$. In Eq. 7, $\circ G_{ij}^{\beta(O)}$ represents the Gibbs energy of a B2 end-member expressed by Eq. 10 with i and j in the first and second sublattices, respectively. $L_{i,j,k}^{\beta(O)}$ is the interaction term between end-members of ij and ik that takes the form of $A + B \times T$ where A and B are the model parameters to be evaluated in modeling process. Relationships between the interaction parameters used in the CEF and partitioned models exist and are derived by Dupin and Ansara [26]. B2 end-members have both sites equivalent to one another so A2 disordering is possible when those sites have the same disordered occupancy. This crystallographic site equivalency is taken into account with the following expressions [26]:

$$\circ G_{ij}^{\beta} = \circ G_{ji}^{\beta}, \quad v L_{i,j,k}^{\beta} = v L_{k,i,j}^{\beta}, \quad v L_{i,j,k,l}^{\beta} = v L_{k,l,i,j}^{\beta}, \quad \text{and} \quad v L_{i,j,k;l}^{\beta} = v L_{l;i,j,k}^{\beta} \tag{Eq.8}$$

As adopted from the Co-Cr binary [17], σ is modeled with the sublattice formulation (Al, Co)₈(Al,Co,Cr)₁₈(Cr)₄. The phase σ contains σ -(Al)₈(Al)₁₈(Cr)₄, σ -(Al)₈(Cr)₁₈(Cr)₄, σ -(Co)₈(Co)₁₈(Cr)₄, σ -(Co)₈(Cr)₁₈(Cr)₄ binary and σ -(Al)₈(Co)₁₈(Cr)₄, σ -(Co)₈(Al)₁₈(Cr)₄ ternary end-members. To extend the solubility of σ from the binary Co-Cr system, Al must be introduced while keeping consistency with the original model for σ . Joubert [29] suggested that Al should only be allowed to mix in the first and second sublattices given its size and electronic characteristics. In accordance with this, a model described as (Al,Co)₈(Al,Co,Cr)₁₈(Cr)₄ is established. The Gibbs energy of σ in per mole of formula has the form,

$$\begin{aligned} G_m^\sigma &= \sum_i \sum_j y_i' y_j'' \circ G_{ij:Cr}^\sigma + RT[8 \sum_i y_i' \ln(y_i') + 18 \sum_j y_j'' \ln(y_j'')] \\ &+ \sum_{i_1} \sum_{i_2} \sum_j \{y_{i_1}' y_{i_2}' y_j'' [\sum_k L_{i_1,i_2;j:Cr}^\sigma (y_{i_1}' - y_{i_2}')^k]\} \\ &+ \sum_i \sum_{j_1} \sum_{j_2} \{y_i' y_{j_1}'' y_{j_2}'' [\sum_k L_{ij_1;j_2:Cr}^\sigma (y_{j_1}'' - y_{j_2}'')^k]\} \end{aligned} \tag{Eq.9}$$

where y_i' and y_i'' represent the site fractions of i in the first and second sublattices, $\circ G_{ij:Cr}^\sigma$ represents the Gibbs energy of particular σ end-members as shown by Eq. 10, and $L_{i,j,k:Cr}^\sigma$ is the interaction term between end-members of $ij:Cr$ and $ik:Cr$.

The described binary and ternary end-members for B2 and σ are modeled as follows,

$$G_m^{Al_xCo_yCr_z} = x^o G_{Al}^{fcc} + y^o G_{Co}^{hcp} + z^o G_{Cr}^{bcc} + \Delta_f G^{Al_xCo_yCr_z} \quad \text{Eq.10}$$

where $\Delta_f G^{Al_xCo_yCr_z} = \Delta_f H^{Al_xCo_yCr_z} - T\Delta_f S^{Al_xCo_yCr_z}$ and represents the Gibbs energy of formation of a particular B2 or σ end-member with the composition $Al_xCo_yCr_z$. The Debye-Grüneisen model is used to predict the enthalpy and entropy of the compounds as a function of temperature from 0 K properties obtained by the DFT calculations. Details for these calculations are presented in the following section. The PARROT module within Thermo-Calc [30] is used to assess all model parameters for each phase in the system using the phase equilibrium data from our experimental measurements and the results by Ishikawa et al. [13] as well as first-principles thermochemical data calculated in the present work. PARROT is a thermodynamic data assessment module which has been developed to fit model parameters to experimental data by a least mean square method [31].

First-principles methodologies

The Helmholtz energy, $F(V, T)$, of a condensed phase, in terms of the quasiharmonic approach, from first-principles calculations based on DFT is expressed as follows [32,33]:

$$F(V, T) = E_{0K}(V) + F_{Vib}(V, T) + F_{T-el}(V, T) \quad \text{Eq.11}$$

In the above expression, $F_{Vib}(V, T)$ and $F_{T-el}(V, T)$ represent the temperature-dependent vibrational and thermal-electronic contributions, respectively. In the present work, the Helmholtz energy is taken approximately as the Gibbs energy due to the negligible ambient pressure used in the modeling. The thermal electronic contribution to the Helmholtz energy is estimated based on the electronic density of states and calculated using Fermi-Dirac statistics for metallic systems [32]. $E_{0K}(V)$ is the static contribution at 0 K without the zero-point vibrational energy. It is obtained using a four-parameter Birch-Murnaghan (BM4) equation of state (EOS) [32,34]:

$$E_{0K}(V) = a + bV^{-2/3} + cV^{-4/3} + dV^{-2} \quad \text{Eq.12}$$

where a , b , c , and d are fitting parameters. Energy versus volume (E-V) data used in the fitting are relaxed with respect to ionic positions and cell shape at the given volumes.

Lattice vibrations are modeled with the Debye-Grüneisen model with the benefit of both accuracy and efficiency; the relevant equations have been described in detail in previous publications [35,36]. The scaling factor is implemented to scale the Debye temperature as a consequence of the differences in transverse and longitudinal phonon modes [37]. It has been shown that the scaling factor is highly dependent on the crystal structure [38,39]. This factor can be estimated from elastic constant calculations using DFT and then averaged as an isotropic medium. Elastic constant calculations are implemented in this work for fcc-Al, hcp-Co, bcc-Co, B2, and σ using the method proposed by Shang et al. [40].

In order to predict A2 solution mixing, calculations of the enthalpy of mixing based on special quasirandom structures calculations (SQS) [41] are performed using the 16-atom binary A2 model developed by Jiang et al. [42] and the 32- or 36-atom ternary A2 model developed by Jiang [43]. Additionally, ternary B2 solution mixing calculations are also performed using 8- and 16-atom supercells generated for the isostructural B2-AlNi system by Jiang et al. [44]. SQS calculation procedures for the present work are performed with the method recently implemented by Lieser et al. [45]. The SQS supercells are first relaxed with respect to cell volume only, and then to only cell volume and shape, and finally to cell volume, shape as well as ion positions simultaneously. Radial distribution functions (RDF) of relaxed supercells are compared

with the ideal bcc structure after each relaxation step [45]. The structures with the lowest energy that retain the required structural symmetry are used in the present work.

The Vienna *ab-initio* Simulation Package (VASP) [46] is used for spin-polarized DFT calculations due to the ferro- and antiferromagnetic natures of Co and Cr, respectively. Electron-ion interactions are described by the accurate projector augmented-wave (PAW) method [47,48]. The generalized gradient approximation (GGA) as implemented by Perdew, Burke, and Ernzerhof (PBE) [49] is used to describe the electron exchange and correlation. A plane-wave cut-off energy of 400 eV is consistently used to ensure enough basis sets are included, as recommended by the VASP manual [50]. Reciprocal k -meshes used for fcc-Al/Co, hcp-Co, bcc-Al/Co/Cr, B2 and σ are $21 \times 21 \times 21$, $23 \times 23 \times 12$, $17 \times 17 \times 17$, $15 \times 15 \times 15$, and $6 \times 6 \times 11$, respectively. The structures are relaxed by implementing the Methfessel-Paxton method [51] to minimize the forces acting on the atoms. After relaxations, a final calculation using the tetrahedron with Blöchl corrections [52] is applied to ensure an accurate total energy calculation.

Results and Discussion

Experimental results

Alloy phase constitutions were determined through a combination of XRD (selected spectra shown in Fig 1) and phase composition analyses (EPMA results given in Table 1). At 1173 and 1273 K, the alloys A4, A5 and A7 are within the B2- γ - σ three-phase triangle, which is an invariant equilibrium in a three-component system. Small differences measured between the phase compositions are larger than the experimental standard deviation, and may reflect the slight influence of Y on phase equilibria. Selected microstructures observed after equilibration at 1273 and 1373 K are shown in Fig 2. In Fig 2A and 2B, the dark matrix is B2, the two light phases are γ and σ , and the bright precipitates are Y-containing intermetallics (denoted MY). These phases are identified based on their measured compositions and associated XRD results. This phase constitution is typical for equilibrium at 1173 and 1273 K. At 1373 K, the B2 phase exhibits compositions that vary widely between the four alloys studied. These are substantially different from those measured at 1173 and 1273 K, with Al contents as low as 16.2 at.% and Cr contents as high as 36.9 at.%. Nevertheless, XRD confirmed that the ordered B2 structure is maintained at 1373 K. In the absence of σ reflections, it is concluded that σ has been replaced by A2, which dissolves significantly more Al (Table 1). The A2 and B2 phases each have a cubic structure, and their peaks cannot be resolved with the instrument available. Analysis by EPMA (not shown here) indicated that two types of Co-rich yttrides were present, containing ~ 7 at.% and ~ 9 at.% Y, with 18–25 at.% Cr and 9–14 at.% Al. Due to the low volume fraction of these phases, their structures could not be determined by XRD.

The present experimental results confirm and refine the phase relationships originally documented by Ishikawa et al. [13]. Between 1273 and 1373 K, the B2+ γ + σ three-phase region is replaced by an A2+B2+ γ triangle, and the solubility of Cr in B2 drastically increases. Both are due to the shrinkage of the A2/B2 miscibility gap as the temperature increases, and to the associated dissolution of σ into A2. Ishikawa et al. [13] observed the A2/B2 order-disorder transition at 1473 K. The present measurements show very close compositions for B2 and A2 in equilibrium with γ at 1373 K and therefore, indicate that the miscibility gap is closed slightly above 1373 K.

First-principles results

To provide a benchmark for the first-principles methodology used in the present work, fundamental properties of Al, Co, Cr and relevant phases, shown in Table 2, are compared with previous first-principles calculations [53,54] and data from various experiments [55–59]. Good

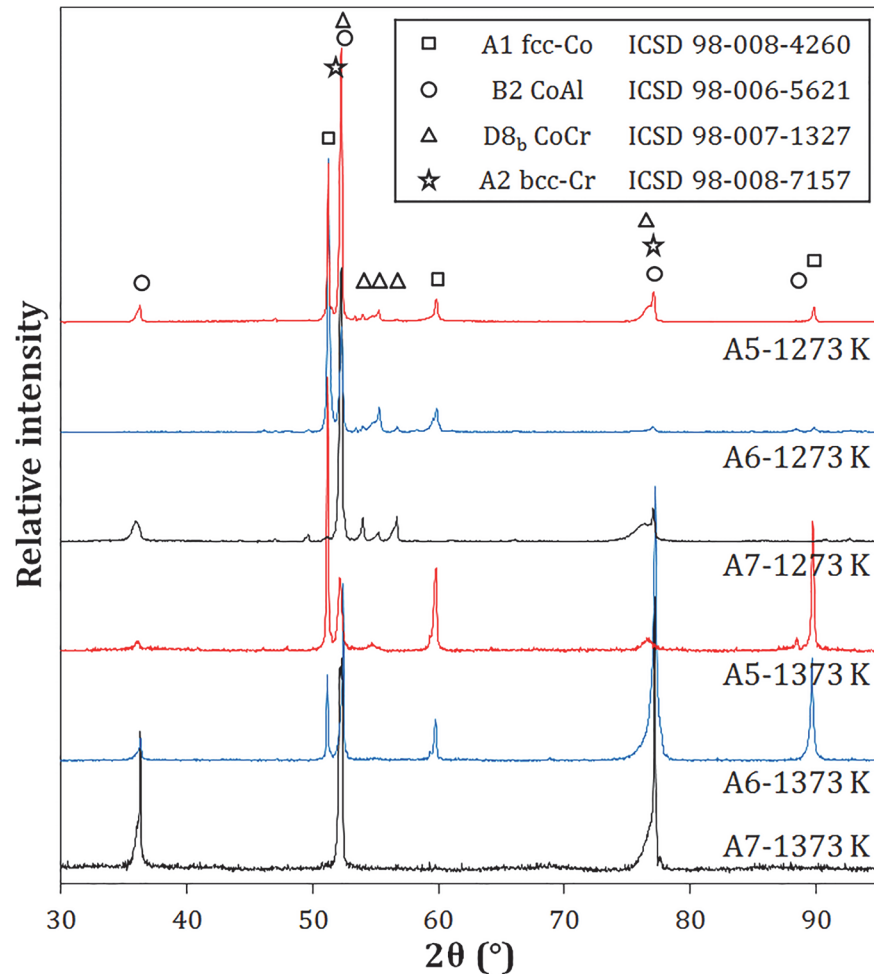


Fig 1. XRD analysis of selected alloy phase constitutions at 1273 K and 1373 K. Note that preferential orientations inherent to cast microstructures were still present after annealing. Specimens were rotated in-plane to ensure that all phases were detected.

doi:10.1371/journal.pone.0121386.g001

agreement is seen for these properties for all three elements in their standard element reference (SER) state (pure, most stable at 298 K and 1 bar) [22]. It should be noted that Cr takes on an anti-ferromagnetic state at 0 K. The results agree with previous calculations and experiments [56,59,60] for anti-ferromagnetic Cr. The lattice parameters and bulk modulus of B2-(Al)(Co) agree with previous results [61,62] and hence, the predicted values for B2-(Co)(Cr) and B2-(Cr)(Al) can be adopted with confidence. No measured bulk moduli for σ -CoCr could be found in the literature and hence, only experimental lattice parameters are compared. The calculated values for the end-members σ -(Co)₈(Co)₁₈(Cr)₄ and σ -(Co)₈(Cr)₁₈(Cr)₄ are compared to the lattice parameter of a σ -Co₁₃Cr₁₇ alloy and are in good agreement with measurements by Dickins et al. [55].

Results from our recent study on the Debye-Grüneisen model [63] indicate that using a calculated scaling factor for the Debye temperature is an accurate and efficient method to predict thermodynamic properties of pure elements and intermetallic phases in comparison with the more computationally demanding phonon supercell approach. Table 2 shows that the pure-element properties derived from the EOS fitting match experiments [56–58] and the DFT predictions [54,60]. Therefore, the Debye approximation is used to estimate the thermodynamic

Table 1. Phase compositions of the CoCrAlY alloys measured by EPMA (at.%).

T (K)	Ref.	B2			γ			σ			A2		
		Al	Cr	Co	Al	Cr	Co	Al	Cr	Co	Al	Cr	Co
1173	A4	36.6	13.2	50.3	5.6	34.3	60.1	2.9	54.0	43.1			
	A5	36.3	13.6	50.1	5.5	34.8	59.7	2.9	54.5	42.6			
	A6	36.3	14.2	49.5	5.5	35.3	59.2	2.9	54.8	42.3			
	A7	36.8	14.6	48.7				2.9	57.4	39.7			
1273	A4	32.0	18.1	49.9	6.6	35.8	57.6	4.0	53.5	42.5			
	A5	31.2	19.2	49.7	6.8	36.2	57.0	4.0	53.8	42.2			
	A6	31.7	18.9	49.5	6.7	36.2	57.1	3.9	54.1	42.0			
	A7	33.1	18.5	48.3				3.8	56.8	39.4			
1373	A4	28.2	20.7	51.1	8.4	33.7	57.9						
	A5	26.0	23.6	50.3	8.4	34.5	57.2						
	A6	16.2	36.9	46.8	8.0	36.5	55.5				12.4	41.6	46.0
	A7	22.3	33.4	44.2							11.7	48.4	39.9

doi:10.1371/journal.pone.0121386.t001

properties for all end-members of B2 and σ . Predicted enthalpies of formation ($\Delta_f H$) for each end-member of B2 and σ are calculated at 298 K and are shown in Table 3. Note that the non-SER reference B2 formation energies are calculated with respect to the bcc phase of the pure elements and that σ energies are taken with respect to the fcc phase in the first sublattice, bcc in the second and bcc in the third following Ref. [7,17]. Experimental thermochemical data for B2 and σ end-members are unavailable at 298 K and consequently, only previous CALPHAD assessments and DFT results are compared in Table 3. Stein et al. [64] determined values of $\Delta_f H_{298} = -64.45$ kJ/mol-atom and $\Delta_f S_{298} = -11.43$ J/mol-atom of B2 based on modeling of experimental enthalpy data at 1100 K. The present DFT predictions using the scaling factor Debye-Grüneisen model are in excellent agreement with these values.

Unfortunately, calorimetric measurements for σ -CoCr have proven unreliable, as reported measured and calculated enthalpies of formation range from -3 to +10 kJ/mol-atom, shown in Ref. [65–67]. Also, the stability of σ in the Co-Cr system was suggested to range from 30 to 45 at.% Co, which is quite different from the calculated end-member compositions of 26.6 and 86.6% at.% Co. However, Downie and Arslan [67] measured the formation enthalpy of one σ -CoCr sample close to the composition of the end-member σ -(Co)₈(Cr)₁₈(Cr)₄ at 473 K and found $\Delta_f H = 6.77$ kJ/mol-atom. While no direct comparison can be made due to the composition and site fractions, the predicted value of $\Delta_f H_{298} = 6.19$ kJ/mol-atom for σ -(Co)₈(Cr)₁₈(Cr)₄ is in good agreement with the measured value. Table 3 shows the final values (non-SER columns) for B2 and σ that are used as input for the thermodynamic modeling in the present work.

For all binary and ternary bcc SQS calculations, RDFs indicate that the simultaneous relaxation of cell volume, shape and ion positions reduce the symmetry of the SQS cell environment. Additionally, ternary SQS calculations show symmetry reduction when only cell volume and shape are allowed to relax. Therefore, SQS supercells with the lowest energy and a coordination environment sufficiently close to the ideal bcc structure are used in the analysis. Calculated binary and ternary enthalpies of mixing are shown in Table 4 and Fig 3 for A2 and B2. Along with the symmetry, the magnetism of the SQS supercells is checked. Cobalt is ferromagnetic at 0 K with an average μ_B /atom of 2.2 while Al is non-magnetic. At 0 K, Cr is antiferromagnetic with no net average magnetic moment. Our calculations show that Al and Cr additions, both with no net magnetic moment, decrease the μ_B /atom of Co as a function of composition.

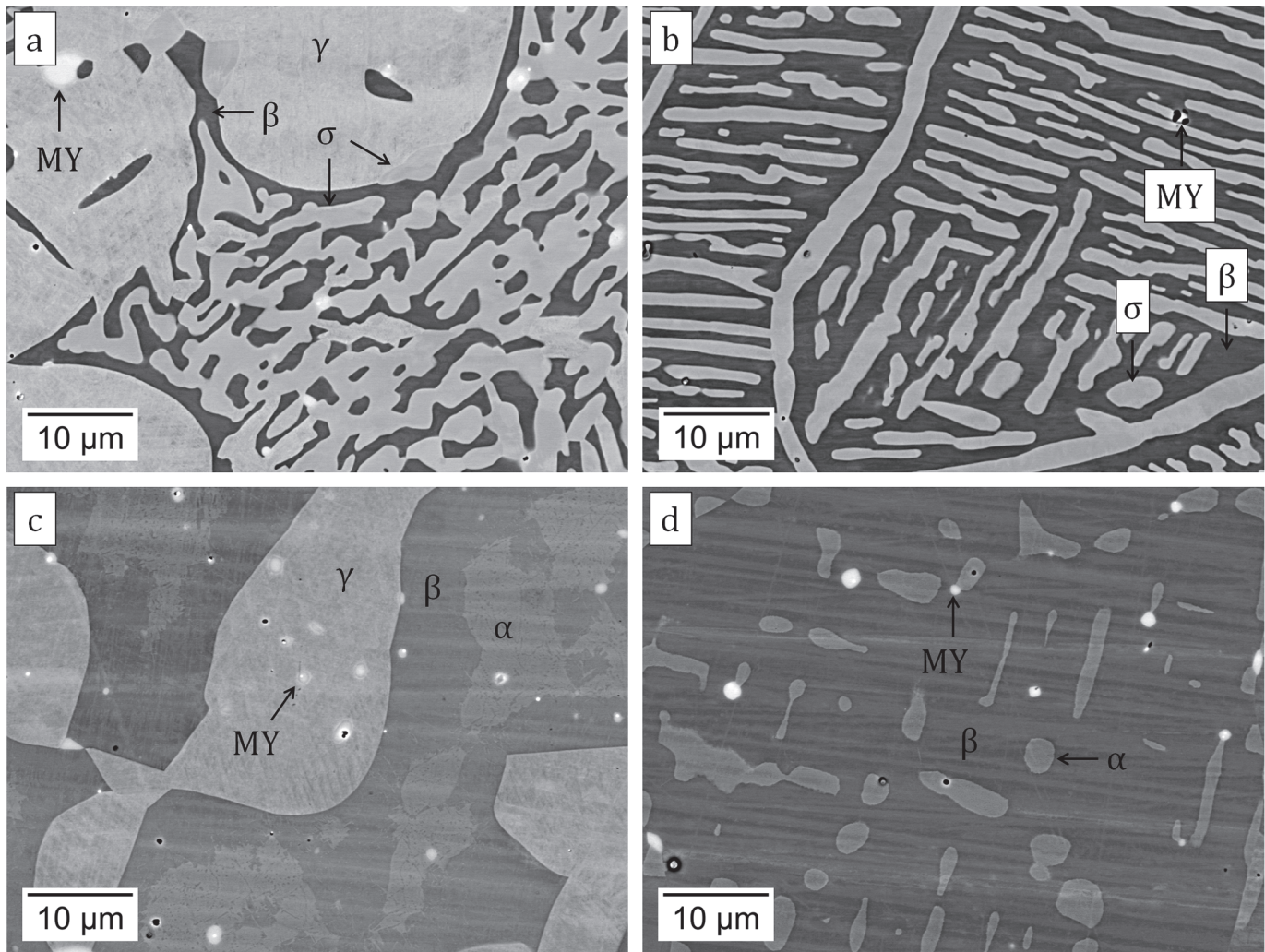


Fig 2. Microstructure of alloys (a,c) A6 and (b,d) A7 equilibrated at (a,b) 1273 K and (c,d) 1373 K. The bright precipitates are Y-containing intermetallics (noted MY).

doi:10.1371/journal.pone.0121386.g002

The SQS calculations, shown in Fig 3 and Table 4, predict the formation of a low-temperature miscibility gap in both Co-Cr and Al-Cr while strong negative mixing is seen in Al-Co. These predictions agree well with experimental observations as well as previous models of the Al-Co [16,64] and Co-Cr [17] binary systems currently adopted for the thermodynamic modeling. In the Co-Cr binary modeled by Oikawa et al. [17], a low temperature A2 miscibility gap is seen at 298 K. Furthermore, the predicted A2 $Al_{0.5}Co_{0.5}$ mixing enthalpy (Table 3) is in good agreement with the Al-Co assessment [16]. However, the Al-Cr model [20] does not produce a low-temperature A2 miscibility gap and hence, disagrees with our current predictions. This is due to a lack of low-temperature thermochemical data available in the literature at the time when Al-Cr was originally modeled. Ternary A2 miscibility gaps are also predicted (Fig 3A), especially along the $Al_{0.5}Co_{0.5}$ -Cr cross-section where the composition $Al_{0.5}Co_{0.5}$ shows the lowest mixing enthalpy on the whole energy surface. A convex energy surface would produce a tangent from $Al_{0.5}Co_{0.5}$ to pure Cr that generates a large miscibility gap across the entire $Al_{0.5}Co_{0.5}$ -Cr cross-section. When B2 mixing is also taken into account, as shown in Fig 3B, this A2 and B2 miscibility gap becomes more prominent across the $Al_{0.5}Co_{0.5}$ -Cr cross-section

Table 2. Various properties of the Al, Co, Cr, and the end-members of B2 and σ .

Phase	V_0 ($\text{\AA}^3/\text{atom}$)	B_0 (GPa)	Scaling factor	Source
Al (fcc)	16.50	78	0.63	Present work
	17.08	65		DFT[54]
		72		Experiment[56]
		79 (0 K)		Experiment[57]
Co (hcp)	10.88	210	0.78	Present work
	11.07	204		DFT[54]
		191		Experiment[56]
		196 (0 K)		Experiment[58]
Cr (bcc)	11.59	176	0.88	Present work
	11.56	189		DFT[60]
	11.58	258		DFT[54]
		190		Experiment[56]
		192 (0 K)		Experiment [59]
B2 Phase				
(Al)(Co)	11.61	178	0.87	Present work
		157		DFT[61]
		162±5		Experiment[61]
(Co)(Cr)	11.60	214	0.77	Present work
(Cr)(Al)	14.03	125	0.82	Present work
σ Phase				
(Al) ₈ (Al) ₁₈ (Cr) ₄	15.70	86	0.78	Present work
(Al) ₈ (Cr) ₁₈ (Cr) ₄	12.36	199	0.82	Present work
(Co) ₈ (Al) ₁₈ (Cr) ₄	13.07	141	0.78	Present work
(Al) ₈ (Co) ₁₈ (Cr) ₄	11.65	174	0.78	Present work
(Co) ₈ (Co) ₁₈ (Cr) ₄	11.12	197	0.69	Present work
(Co) ₈ (Cr) ₁₈ (Cr) ₄	11.33	249	0.75	Present work

These properties are derived from the energy vs. volume curves using the 4-parameter Birch-Murnaghan EOS. B_0 denotes the bulk modulus. The bulk modulus at room temperature of Al, Co, and Cr are also presented, as reported by Kittel [56]. Other experimental temperatures are shown if known; reported 0 K values are extrapolated from low temperature data.

doi:10.1371/journal.pone.0121386.t002

in accordance with the experiments by Ishikawa et al. [13]. The extremely high formation energy of the end-member (Al)(Co) is responsible for this behavior. Additionally, the SQS results show that A2 is more stable than B2 near Cr because $\Delta H_{mix} = -1.17$ kJ/atom for A2 at the composition $\text{Al}_{0.25}\text{Co}_{0.25}\text{Cr}_{0.5}$ while $\Delta H_{mix} = 8.22$ kJ/atom for B2 at the same composition. These SQS results are in good agreement with measured phase compositions by Ishikawa et al. [13] as well as the present experimental findings. As shown later in Fig 4, this A2/B2 miscibility gap is still observed at 1173 K.

CALPHAD modeling results

The three binary models, Al-Co [16], Co-Cr [17], and Al-Cr [20], are extrapolated to the ternary system using the partitioning model [26]. In addition, thermodynamic parameters from DFT, listed in Table 3, are used as input. The binary B2-(Al)(Co), B2-(Cr)(Al), σ -(Co)₈(Co)₁₈(Cr)₄ and σ -(Co)₈(Cr)₁₈(Cr)₄ end-members are fixed by previous models and cannot be modified without reassessment of those systems. The initial ternary extrapolation produces a phase diagram with satisfactory phase boundaries for fcc, A2, and B2 at 1173 K compared to experiments,

Table 3. Predicted enthalpies and entropies of formation of B2 and σ end-members at 298 K.

Phase	End-member	$\Delta_f H$ (kJ/mol-atom)	$\Delta_f H$ (SER) (kJ/mol-atom)	$\Delta_f S$ (J/mol-a)	$\Delta_f S$ (SER) (J/mol-a)	Source
(B2)	(Al)(Co)	-66.89	-57.67	-13.73	-8.23	Present work
Binary		-64.45		-11.43		CALPHAD[64]
	(Co)(Cr)	11.98	16.60	-1.73	1.03	Present work
	(Cr)(Al)	-7.37	-2.78	-9.18	-6.45	Present work
(σ)	(Co)₈(Al)₁₈(Cr)₄	-30.56	-24.58	-7.33	-4.05	Present work
Ternary	(Al)₈(Co)₁₈(Cr)₄	-18.93	-13.39	-4.44	-1.13	Present work
(σ)	(Co) ₈ (Co) ₁₈ (Cr) ₄	3.60	9.62	0.28	3.60	Present work
Binary	0 K		9.84			Present work
	0 K		11.65			DFT[65]
	(Co) ₈ (Cr) ₁₈ (Cr) ₄	5.72	6.19	0.16	0.16	Present work
	0 K		6.20			Present work
	0 K		8.39			DFT[65]
	(Al) ₈ (Al) ₁₈ (Cr) ₄	5.73	11.24	-6.02	-2.74	Present work
	(Al) ₈ (Cr) ₁₈ (Cr) ₄	1.84	1.84	-3.32	-3.32	Present work

Energies are shown in units of J/mol-formula and atom with the most stable end-members shown in bold text. Also, energies taken with respect to standard states are denoted with SER. Energies used for CALPHAD modeling are taken with different reference states depending on the sublattice models used. B2 formation energies are calculated with respect to the bcc phase of the pure elements. For σ , energies are taken with respect to the fcc phase in the first sublattice, bcc in the second and bcc in the third; same as the sublattice model implemented in the current work.

doi:10.1371/journal.pone.0121386.t003

but is at variance with the experimental isothermal sections at all other temperatures [13,68]. A2/B2 regions do not separate at the order/disorder compositions even at temperatures as high as 1623 K, which is at significant variance with experiments (see [experimental](#) Section 6.1 for discussion). The poor extrapolation is a result of fixing the B2-(Cr)(Al) end-member to the value proposed by Dupin et al. [7] in their modeling of the Al-Cr-Ni ternary system. Dupin et al. [7] assessed $\Delta_f H$ of B2-(Cr)(Al) to be -13.719 kJ/mol-atom, which is much more stable than the value of -7.37 kJ/mol-atom predicted by DFT in the present work. However, modifying this energy will require significant reassessment of Al-Cr-Ni ternary description and is outside the scope of this work. As a consequence of this fixed B2 end-member, additional interaction parameters for the B2 phase are needed to correctly reproduce its miscibility gap.

The binary B2-(Co)(Cr) end-member and the Co-Cr interaction parameters are evaluated by fitting to the present EPMA results at 1173, 1273, and 1373 K (Table 1) data from Ishikawa et al. [13] as well as first-principles thermochemical data. Given the complexity of the A2/B2 miscibility gap region, as seen in Figs 4–8, ternary, temperature dependent interaction parameters are needed to describe the B2-(Al)(Co) extension into the ternary as well as the A2/B2 transition temperatures. Interaction parameters for the A2 are also needed to capture the Al and Co solubility. The evaluated parameters are shown in Table 5 and built into a thermodynamic database, which can be found in S1 Dataset.

Fig 4 shows the calculated isothermal section at 1173 K compared with the present EPMA results as well as experimental data from Moskvitina et al. [68]. A good agreement between calculations and experiments is reached. Fig 5 shows the calculated isothermal section at 1273 K, which agrees very well with the present experiments as well as measurements by Ishikawa et al. [13]. Fig 6 shows a calculated isothermal section at 1373 K, which agrees well with our experiments, except for the B2 composition in the A2+B2+ γ three phase tie-triangle and the A2-B2 tie-line. This is attributed to the fact that the A2/B2 miscibility gap disappears very rapidly with increasing temperature, and as a consequence the morphology of this region of the

Table 4. Calculated enthalpies of mixing for solution A2 and B2.

Al	Co	Cr	SQS prototype	ΔH_{mix} (kJ/mol-atom)
A2				
Al-Co				
0.75	0.25		16	-8.71
0.5	0.5		16	-21.69
0.25	0.75		16	-18.57
Co-Cr				
	0.75	0.25	16	9.99
	0.5	0.5	16	11.98
	0.25	0.75	16	9.59
Al-Cr				
0.75		0.25	16	2.45
0.5		0.5	16	1.44
0.25		0.75	16	1.01
Al-Co-Cr				
0.5	0.25	0.25	32	-9.36
0.25	0.5	0.25	32	-6.86
0.25	0.25	0.5	32	-1.17
0.33	0.33	0.33	36	-7.86
Al	Co	Cr	SQS prototype	ΔH_{mix} (kJ/mol-atom)
B2				
(Al)(Co)-(Co)(Cr) section				
0.5	0.5	0		-67.75
0.375	0.5	0.125	32	-47.66
0.25	0.5	0.25	8	-27.20
0.125	0.5	0.375	32	-9.96
0	0.5	0.5		11.99
(Co)(Cr)-(Cr)(Al) section				
0	0.5	0.5		11.99
0.25	0.25	0.5	8	8.22
0.5	0	0.5		-7.96
(Cr)(Al)-(Al)(Co) section				
0.5	0	0.5		-7.96
0.5	0.125	0.375	32	-18.49
0.5	0.25	0.25	8	-32.77
0.5	0.375	0.125	32	-49.54
0.5	0.5	0		-67.75

These calculations are based on binary and ternary SQS calculations at 0 K with references taken as bcc-A2 for Al, Co, and Cr.

doi:10.1371/journal.pone.0121386.t004

diagram is extremely sensitive to temperature variations around 1373 K. The A2+B2+ γ three phase triangle is predicted to disappear at 1423 K measurements by Ishikawa et al. [13] at 1473 K. Fig 7 plots the 1473 K isothermal section, which fits experimental measurements from Ishikawa et al. [13] quite well. At this temperature, the A2/B2 miscibility gap is replaced by a second-order transition represented by a dotted line. The calculation near the transition region shows that the B2 ordering gravitates towards the disordered composition with more Cr additions on the Co-Cr rich side of the phase diagram. This is in good agreement with the

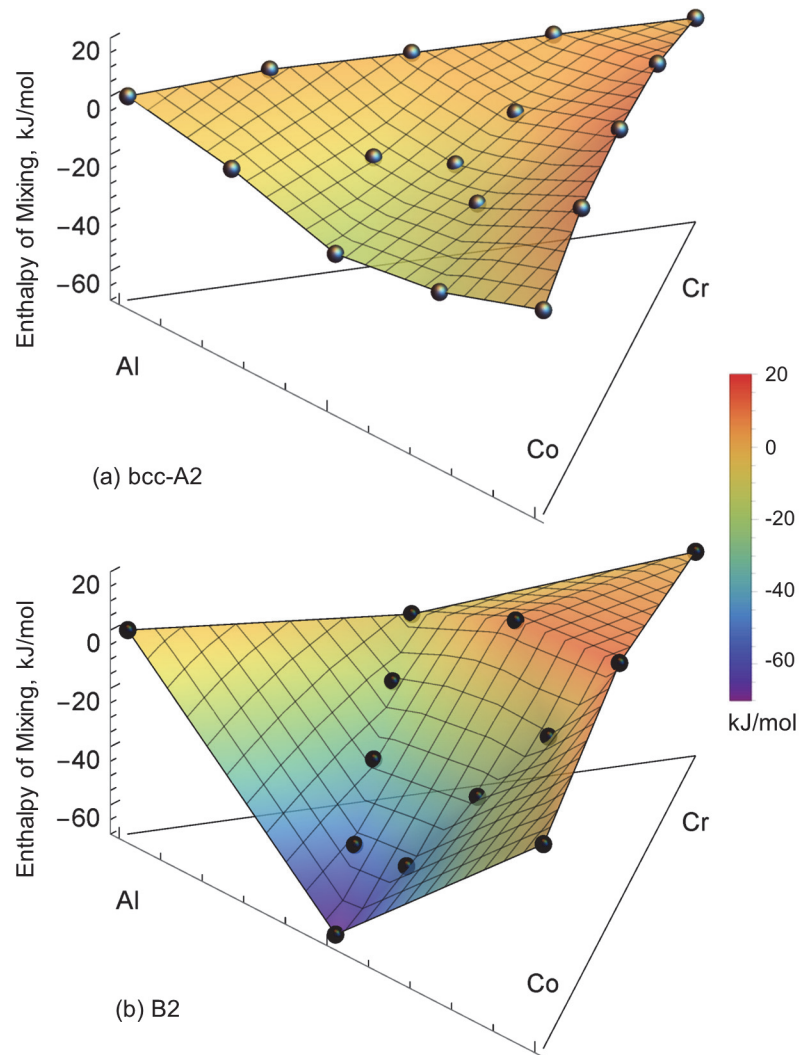


Fig 3. Predicted A2 (a) and B2 (b) enthalpies of mixing. These calculations are based on 16-atom binary and 32/36-atom ternary SQS supercells at 0 K. Grey points in (a) represent distinct A2 SQS compositions and black points in (b) represent B2 SQS compositions. A color map is added to guide the reader in viewing the energy surface.

doi:10.1371/journal.pone.0121386.g003

experimental results on the order/disorder alloys found by Ishikawa et al. [13]. Fig 8 shows the 1573 K isothermal sections. Furthermore, the A2/B2 and B2/ γ tie-lines as well as A2/B2 transition points show good agreement at 1573 and 1623 K compared with data from Ishikawa et al. [13] (not included here). An overall good thermodynamic description of Al-Co-Cr, which takes into account predicted first-principles thermochemical data, is produced in this work. We have demonstrated a model that is able to reproduce the rapid replacement of one three-phase σ +B2+ γ tie-triangle by another and the sharp increase in the solubility of Cr in B2 from 1273 to 1373 K, as observed experimentally (see Section 6.1).

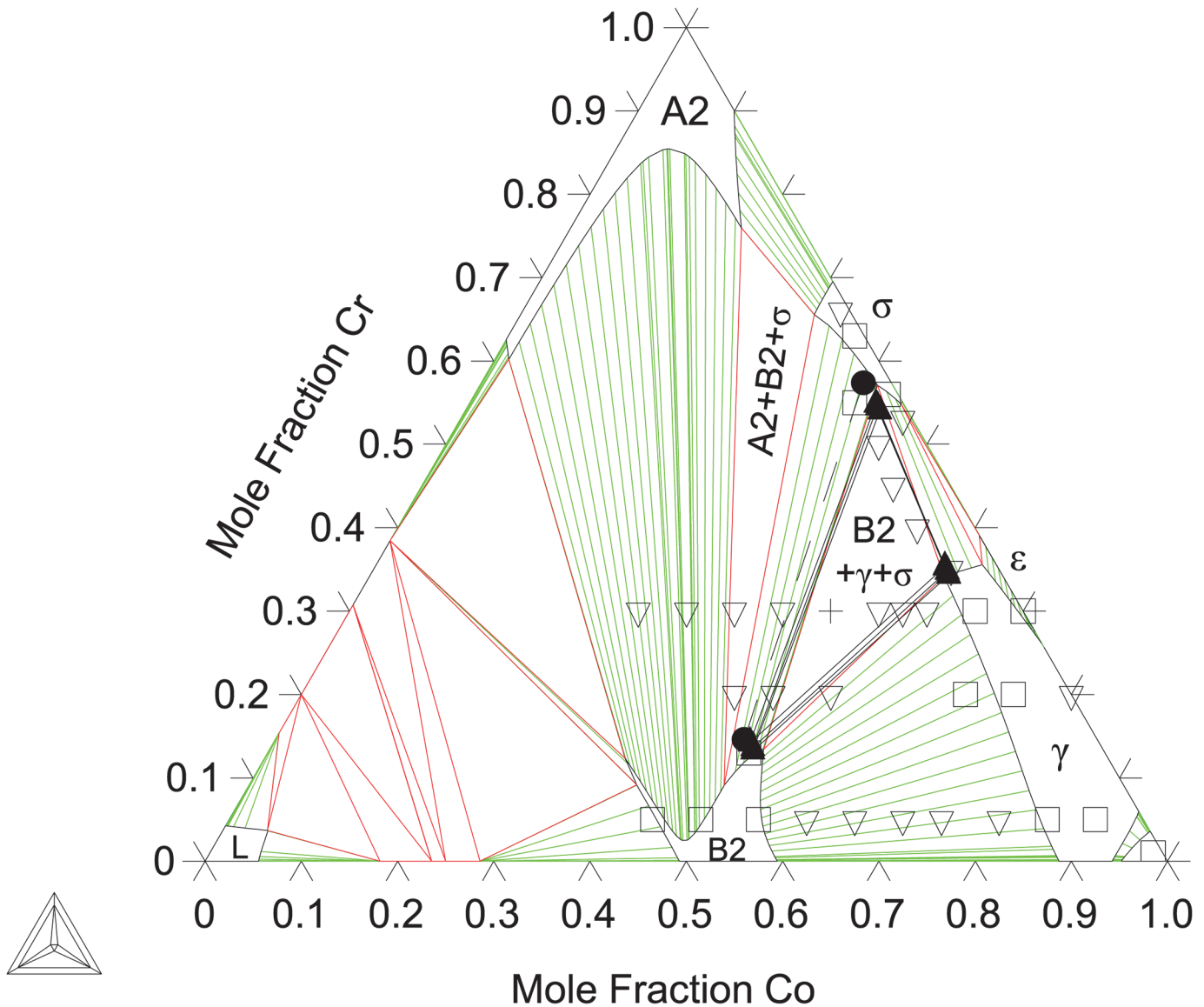


Fig 4. Al-Co-Cr Isothermal section at 1173 K. Shown with phase equilibria data from Moskvitina et al. [68]: single phase (\square), 2-phase (∇), and 3-phase (\blacktriangle). Phase equilibria data from the present work: 2-phase (\bullet), 3-phase (\blacktriangle).

doi:10.1371/journal.pone.0121386.g004

Conclusions

The Al-Co-Cr system is investigated thoroughly using first-principles calculations, XRD, and EPMA measurements to produce a complete CALPHAD thermodynamic description. First-principles DFT calculations predict a large A2/B2 miscibility gap in the ternary system, which is demonstrated experimentally using phase composition measurements from 1173 to 1373 K. In addition, the experimentally-measured phase compositions for A2, B2, γ and σ are in good agreement with previous experimental results [13]. To aid in the modeling of the ternary system, the Debye-Grüneisen model is used to predict finite-temperature data of B2 and σ such as heat capacities, entropies, and enthalpies. It is found that the complex A2/B2 phase region, which includes an order-disorder transition, can be accurately described with a partitioned bcc model. The calculated B2 ordering compositions are also shown to be in agreement with

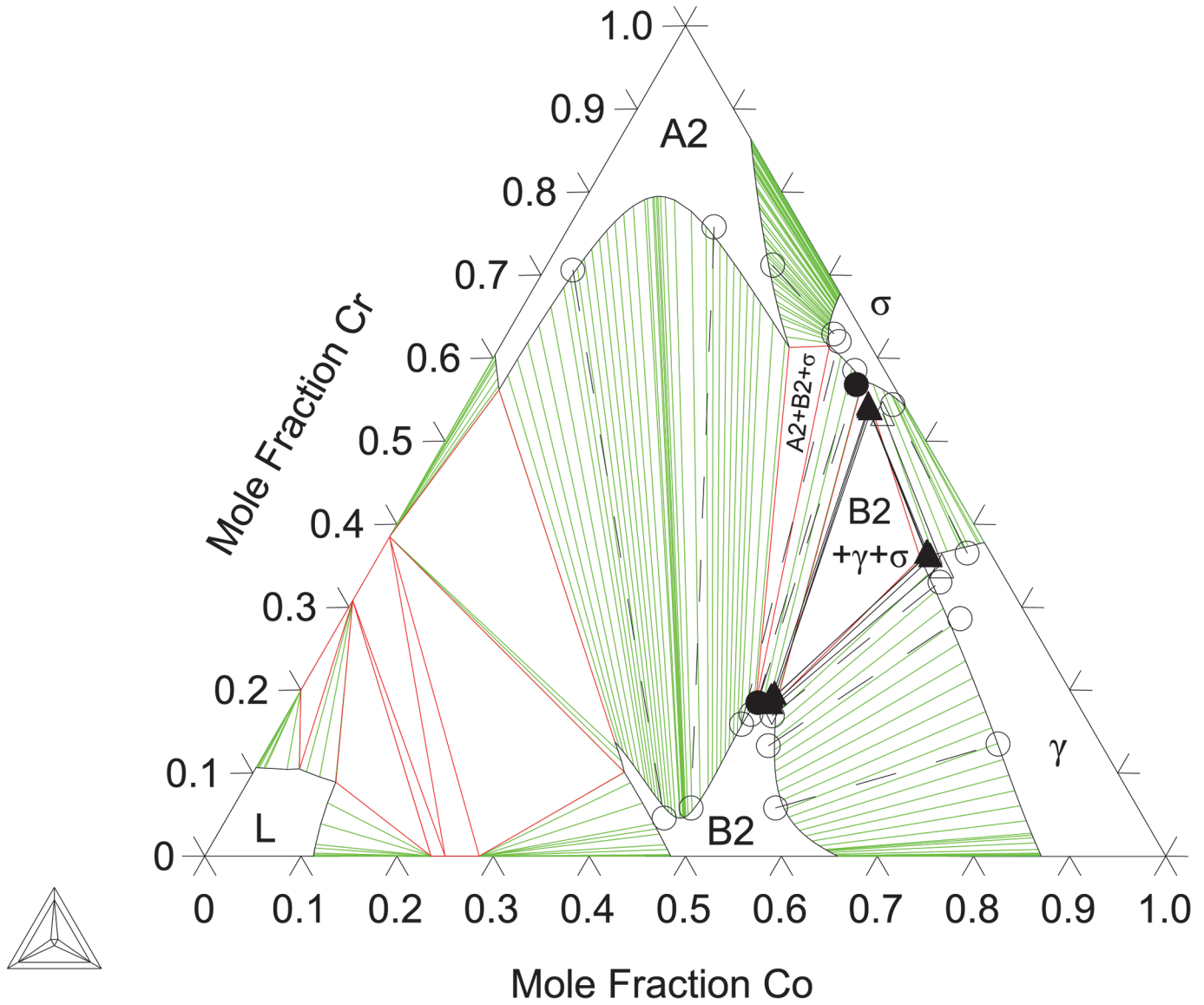


Fig 5. Al-Co-Cr Isothermal section at 1273 K. Shown with phase equilibria data from Ishikawa et al. [13]: 2-phase (○), and 3-phase (△). Experimental phase equilibria data from the present work: 2-phase (●), 3-phase (▲).

doi:10.1371/journal.pone.0121386.g005

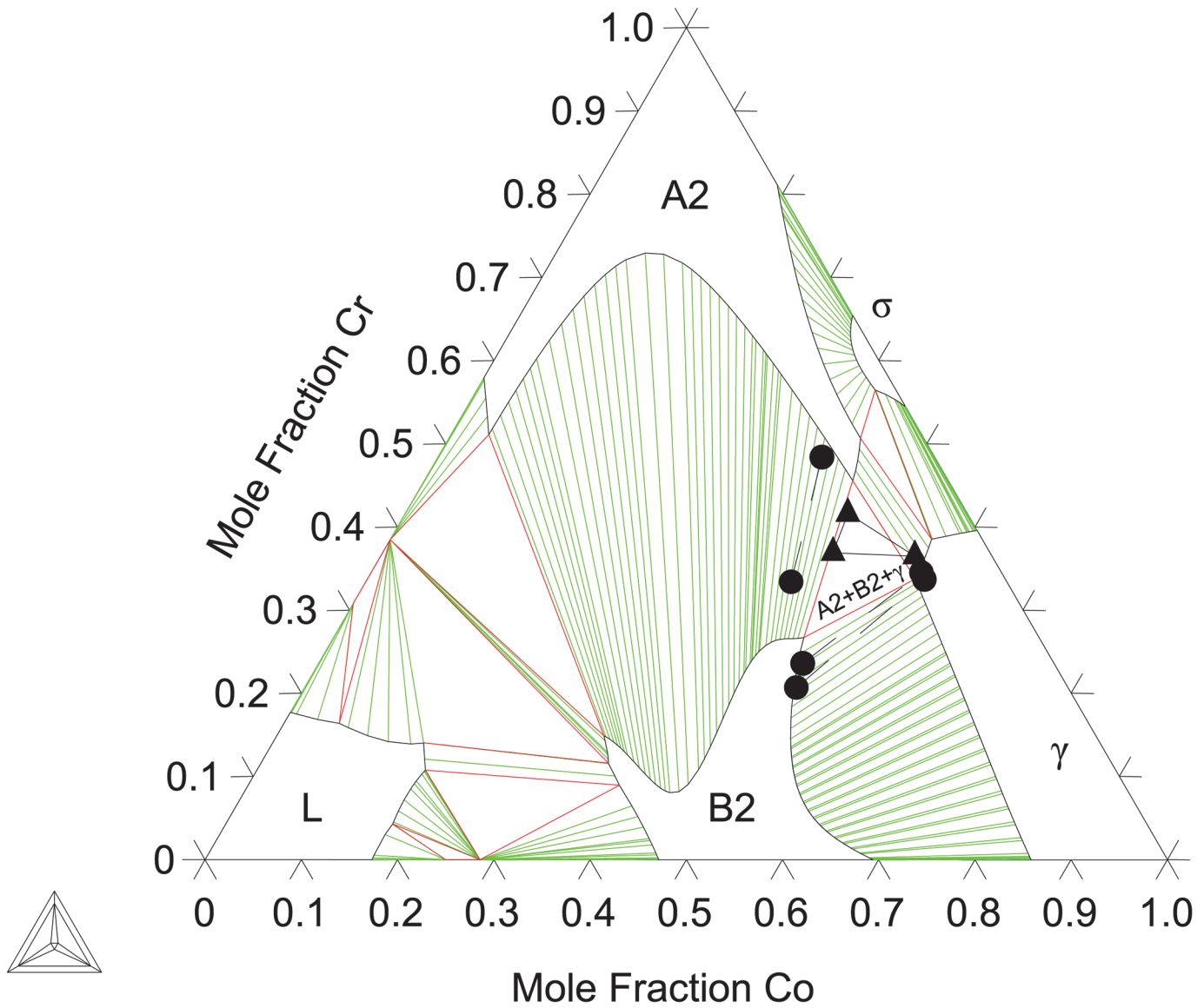


Fig 6. Al-Co-Cr Isothermal section at 1373 K. Shown with phase equilibria data from the present work: 2-phase (●), 3-phase (▲).

doi:10.1371/journal.pone.0121386.g006

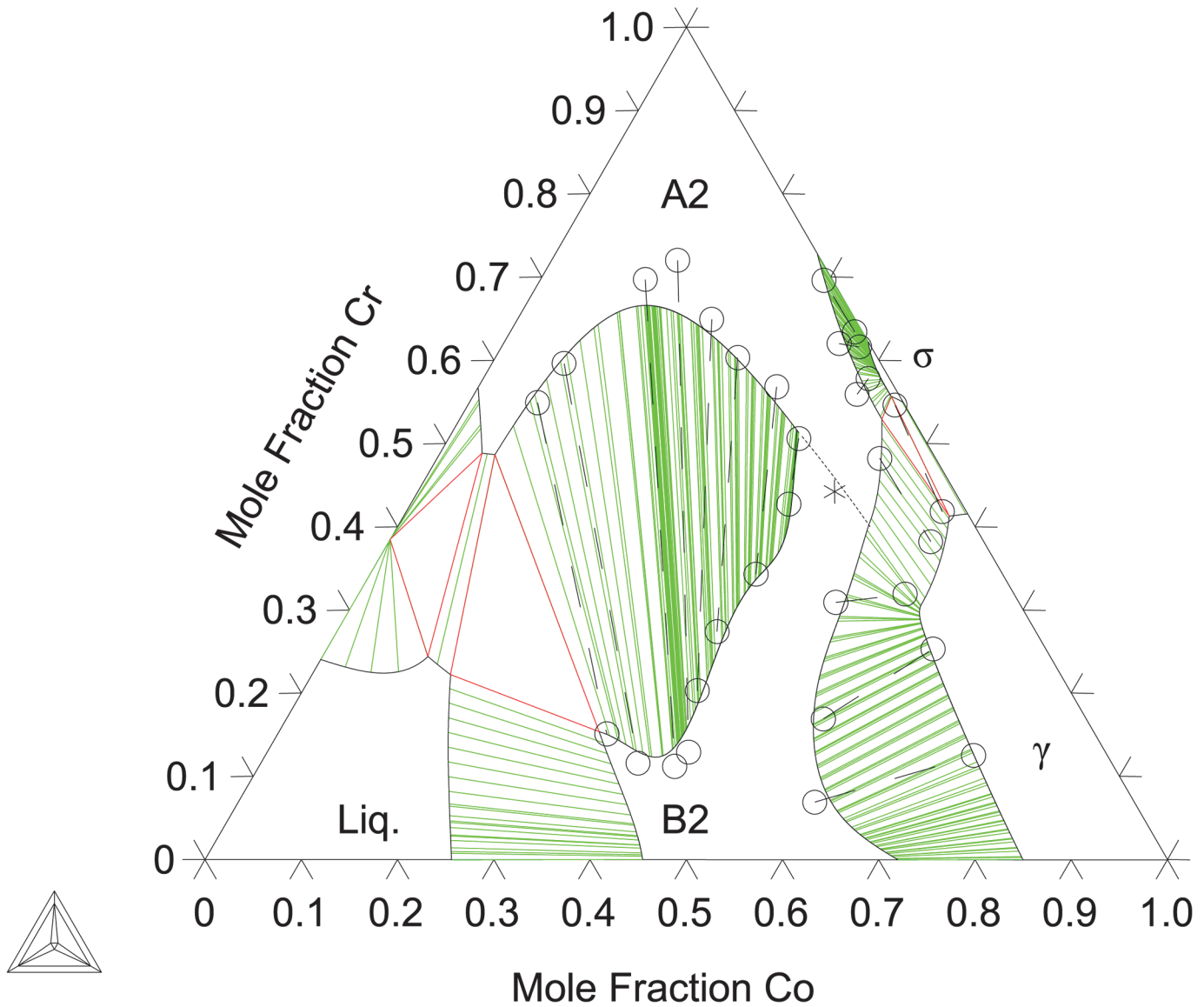


Fig 7. Al-Co-Cr isothermal section at 1473 K. Phase equilibria data from Ishikawa et al. [13]: 2-phase (○), order-disorder transition (*). The calculated order-disorder transition is shown with (- -).

doi:10.1371/journal.pone.0121386.g007

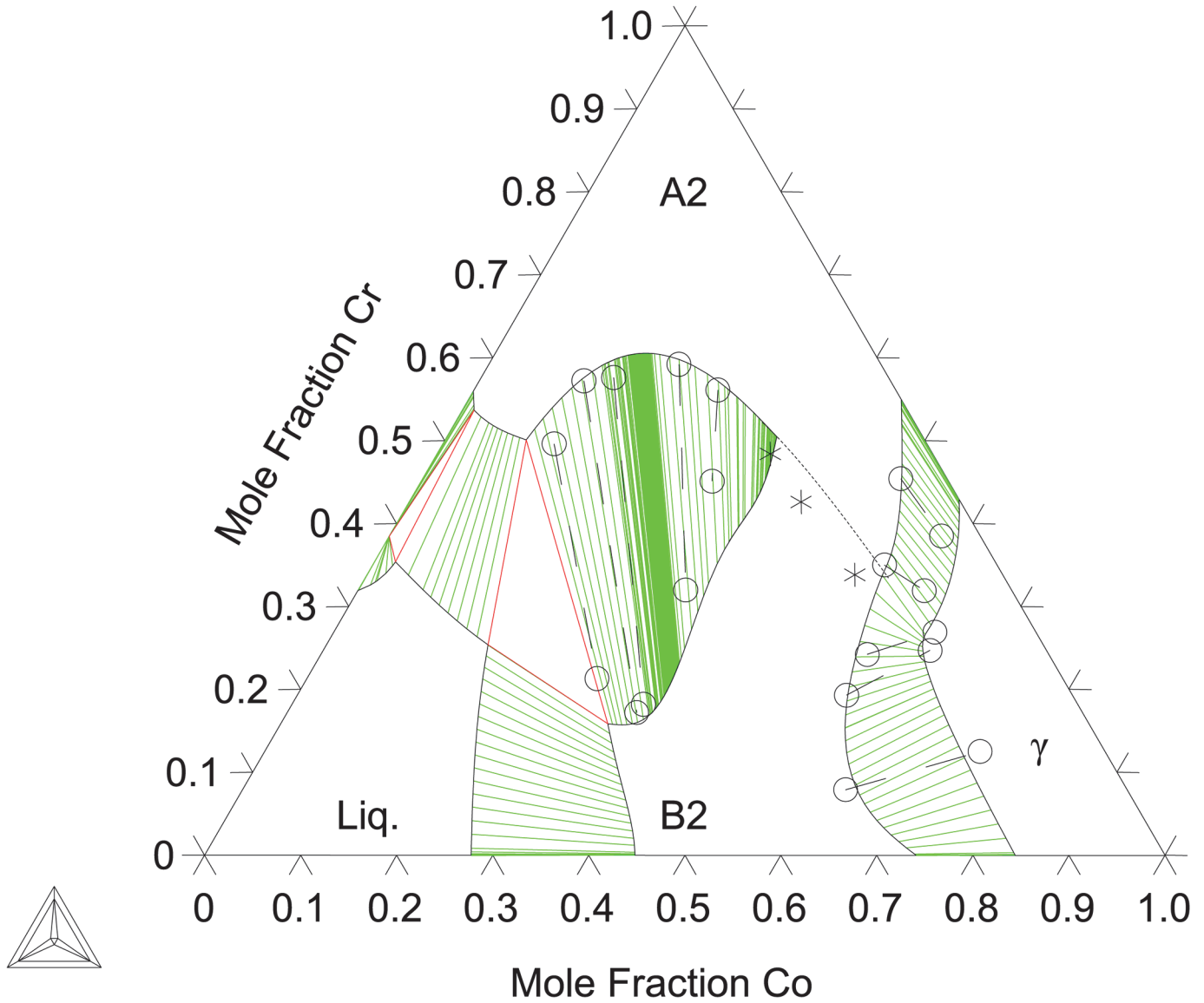


Fig 8. Al-Co-Cr Isothermal section at 1573 K. Phase equilibria data from Ishikawa et al. [13]: 2-phase (□), order-disorder transition (*). The calculated order-disorder transition is shown with (-.-).

doi:10.1371/journal.pone.0121386.g008

Table 5. Model parameters and functions for the ternary Al-Co-Cr system.

Phase	Parameters	Values	References	
liquid (L) phase: (Al,Co,Cr) ₁	${}^0L_{Al,Co,Cr}^{Liq}$	+30000	Present work	
fcc (γ) phase: (Al,Co,Cr) ₁	${}^0L_{Al,Co,Cr}^{fcc}$	+17295	Present work	
hcp (ϵ) phase: (Al,Co,Cr) ₁	${}^0L_{Al,Co,Cr}^{hcp}$	+25000	Present work	
bcc (A2) phase: (Al,Co,Cr,Va) ₁	${}^0L_{Al,Co}^{A2}$	+GB2ALCO–LB2ALCO	Present work	
	${}^0L_{Al,Cr}^{A2}$	–54900 + 10 × T	COST 507[20]	
	${}^0L_{Co,Cr}^{A2}$	+1033–1.481 × T	Oikawa et al.[17]	
	${}^1L_{Co,Cr}^{A2}$	+11972–13.374 × T	Oikawa et al.[17]	
	${}^0L_{Al,Va}^{A2}$	+GB2ALVA–LB2ALVA	Dupin et al.[7]	
	${}^0L_{Co,Va}^{A2}$	+GB2COVA–LB2COVA	Present work	
	${}^0L_{Cr,Va}^{A2}$	+100000	Dupin et al.[7]	
	${}^0L_{Al,Co,Cr}^{A2}$	–LB2ALCO + LBALCOMCR + LBCOCRMAL +L1BCRALMCO	Present work	
	${}^1L_{Al,Co,Cr}^{A2}$	+LALCO2CR–LB2ALCO +LBALCOMCR + LBCOCRMAL	Present work	
	${}^2L_{Al,Co,Cr}^{A2}$	–LB2ALCO + LBALCOMCR +LBCOCRMAL –L1BCRALMCO	Present work	
	beta (B2) phase: (Al,Co,Cr,Va) _{0.5} (Al,Co,Cr, Va) _{0.5}	${}^0G_{Al,Co}^{B2} = {}^0G_{Co,Al}^{B2}$	+0.5 × GB2ALCO–0.5 × LB2ALCO	Present work
		$TC_{Al,Co}^{B2} = TC_{Co,Al}^{B2}$	–1450	Present work
$BMAG_{Al,Co}^{B2} = BMAG_{Co,Al}^{B2}$		–1.35	Present work	
${}^0G_{Co,Cr}^{B2} = {}^0G_{Cr,Co}^{B2}$		+0.5 × GB2COCR	Present work	
${}^0G_{Cr,Al}^{B2} = {}^0G_{Al,Cr}^{B2}$		+0.5 × GB2CRAL	Present work	
${}^0G_{Al,Va}^{B2} = {}^0G_{Va,Al}^{B2}$		+0.5 × GB2ALVA–0.5 × LB2ALVA	Present work	
${}^0G_{Co,Va}^{B2} = {}^0G_{Va,Co}^{B2}$		+0.5 × GB2COVA–0.5 × LB2COVA	Present work	
${}^0G_{Cr,Va}^{B2} = {}^0G_{Va,Cr}^{B2}$		0	Present work	
${}^0L_{Co,Cr,Al}^{B2} = {}^0L_{Al,Co,Cr}^{B2}$		+0.5 × LBCOCRMAL	Present work	
${}^0L_{Al,Cr,Co}^{B2} = {}^0L_{Co,Al,Cr}^{B2}$		+0.5 × LBCRALMCO	Present work	
${}^0L_{Al,Co,Cr}^{B2} = {}^0L_{Cr,Al,Co}^{B2}$		+0.5 × LBALCOMCR + BU1ALCO	Present work	
${}^1L_{Co,Cr,Al}^{B2} = {}^1L_{Al,Co,Cr}^{B2}$		+0.5 × L1BCOCRMAL	Present work	
${}^1L_{Al,Cr,Co}^{B2} = {}^1L_{Co,Al,Cr}^{B2}$		+0.5 × L1BCRALMCO	Present work	
${}^1L_{Al,Co,Cr}^{B2} = {}^1L_{Cr,Al,Co}^{B2}$		+0.5 × L1BALCOMCR	Present work	
${}^0L_{Al,Co,Cr,Al}^{B2} = {}^0L_{Al,Al,Co,Cr}^{B2}$		+0.5 × LAL2COCR	Present work	
${}^0L_{Al,Co,Cr,Co}^{B2} = {}^0L_{Co,Al,Co,Cr}^{B2}$		+0.5 × LALCO2CR	Present work	
${}^0L_{Al,Co,Cr,Cr}^{B2} = {}^0L_{Cr,Al,Co,Cr}^{B2}$		+0.5 × LALCOCR2	Present work	
sigma (σ) phase: (Al,Co) ₈ (Al,Co,Cr) ₁₈ (Cr) ₄		${}^0G_{Al,Al,Cr}^{\sigma}$	+161148	Present work
	${}^0G_{Al,Cr,Cr}^{\sigma}$	+47886	Present work	
	${}^0G_{Co,Co,Cr}^{\sigma}$	–16899–29.814 × T	Oikawa et al.[17]	
	${}^0G_{Co,Cr,Cr}^{\sigma}$	–259935 + 85.097 × T	Oikawa et al.[17]	
	${}^0G_{Al,Co,Cr}^{\sigma}$	–617537	Present work	
	${}^0G_{Co,Al,Cr}^{\sigma}$	–931862	Present work	
	${}^0L_{Co,Al,Cr,Cr}^{\sigma}$	–195992	Present work	
	Function	Value		
LAL2COCR		0	Present work	
LALCO2CR		–78970 + 89.123 × T	Present work	
LALCOCR2	0	Present work		

(Continued)

Table 5. (Continued)

Phase	Parameters	Values	References
<i>LBCOCRMAL</i>		$28320 - 16.474 \times T$	Present work
<i>LBCRALMCO</i>		0	Present work
<i>LBALCOMCR</i>		-46432	Present work
<i>L1BCOCRMAL</i>		0	Present work
<i>L1BCRALMCO</i>		13276	Present work
<i>L1BALCOMCR</i>		0	Present work
<i>GB2ALCO</i>		$-138500 + 34.620 \times T$	Dupin and Ansara [16]
<i>LB2ALCO</i>		$54531 - 37.04 \times T$	Present work
<i>GB2COCR</i>		$35909 - 16.474 \times T$	Present work
<i>GB2CRAL</i>		-4000	Dupin et al.[7]
<i>BU1XY</i> (X,Y = Al,Co,Cr)		$-0.5 \times LB2XY$	Present work

Only A2, B2, and σ binary parameters are listed in full for their importance, all other binary parameters can be found in the respective binary Al-Co[16], Co-Cr[17], and Al-Cr[20] references as well as the attached database file. Parameters are in units of J/mol-formula.

doi:10.1371/journal.pone.0121386.t005

previous as well as present experimental studies. Overall, a consistent thermodynamic description of the Al-Co-Cr system is produced and its accuracy for predicting thermodynamic properties of all phases relevant for MCrAl-base coatings is confirmed.

Supporting Information

S1 Dataset. Thermodynamic database for the Al-Co-Cr system. This dataset contains the models and parameters built using Thermo-Calc for the Al-Co-Cr alloy system in text format. (TXT)

Acknowledgments

Computing clusters LION and Cyberstar are provided by the Materials Simulation Center and the Research Computing and Cyberinfrastructure Group at the Pennsylvania State University. Additionally, this work used the Extreme Science and Engineering Discovery Environment (XSEDE), which is supported by National Science Foundation grant number ACI-1053575. We would like to also thank Dr. Yi Wang and Richard Otis for stimulating discussions about the computational aspects of this work.

Author Contributions

Conceived and designed the experiments: XLL TG BG ZKL. Performed the experiments: XLL TG. Analyzed the data: XLL TG BL GL BG ZKL. Contributed reagents/materials/analysis tools: TG BG ZKL. Wrote the paper: XLL TG BL GL BG ZKL. Implementing the thermodynamic model: BL.

References

1. Wood JH, Goldman E, in Sims CT, Stoloff NSWCH. Superalloys II. 2nd ed. New York, NY: Wiley-Interscience; 1987.
2. Reed RC. The Superalloys. 1st ed. Cambridge, UK: Cambridge University Press; 2006.
3. Goward GW. Progress in coatings for gas turbine airfoils. Surf Coatings Technol. 1998 Oct; 108–109:73–9.

4. Clarke DR, Levi CG. Materials Design for the Next Generation Thermal Barrier Coatings. *Annu Rev Mater Res*. 2003; 33:383–417.
5. Darolia R. Thermal barrier coatings technology: critical review, progress update, remaining challenges and prospects. *Int Mater Rev*. 2013 Aug 18; 58(6):315–48.
6. Evans AG, Mumm DR, Hutchinson JW, Meier GH, Pettit FS. Mechanisms controlling the durability of thermal barrier coatings. *Prog Mater Sci*. 2001 Jan; 46(5):505–53.
7. Dupin N, Ansara I, Sundman B. Thermodynamic Re-Assessment of the Ternary System Al-Cr-Ni. *Calphad*. 2001; 25(2):279–98.
8. Kattner UR. Construction of a Thermodynamic Database for Ni-Base Superalloys: A Case Study. TMS: CALPHAD and Alloy Thermodynamics. 2002.
9. Achar DRG, Munoz-Arroyo R, Singheiser L, Quadackers WJ. Modelling of phase equilibria in MCrAlY coating systems. *Surf Coatings Technol*. 2004 Oct; 187(2–3):272–83.
10. Toscano J, Gil A, Hüttel T, Wessel E, Naumenko D, Singheiser L, et al. Temperature dependence of phase relationships in different types of MCrAlY-coatings. *Surf Coatings Technol*. 2007 Dec; 202(4–7):603–7.
11. Nicholls JR. Designing oxidation-resistant coatings. *JOM*. 2000 Jan; 52(1):28–35.
12. Wright IG, Gibbons TB. Recent developments in gas turbine materials and technology and their implications for syngas firing. *Int J Hydrogen Energy*. 2007 Nov; 32(16):3610–21.
13. Ishikawa K, Ise M, Ohnuma I, Kainuma R, Ishida K. Phase Equilibria and Stability of the BCC Aluminide in the Co-Cr-Al System. *Ber Bunsenges Phys Chem*. 1998; 102:1206–10.
14. Liu Z-K. First-Principles Calculations and CALPHAD Modeling of Thermodynamics. *J Phase Equilibria Diffus*. 2009 Sep 3; 30(5):517–34.
15. Dupin N. Contribution à l'évaluation thermodynamique des alliages polyconstitués à base de nickel (Ph.D. Thesis). INP Grenoble; 1995.
16. Dupin N, Ansara I. Thermodynamic Assessment of the System Al-Co. *Rev Métallurgie*. 1998; 95(9):1121–9. PMID: [21267112](#)
17. Oikawa K, Qin G-W, Ikeshoji T, Kainuma R, Ishida K. Direct evidence of magnetically induced phase separation in the fcc phase and thermodynamic calculations of phase equilibria of the Co-Cr system. *Acta Mater*. 2002 May; 50(9):2223–32.
18. Havrankova J, Vrestal J, Tomiska J. Mass-spectrometric determination of thermodynamic properties of liquid Co-Cr alloys. *Kov Mater*. 1999; 37:34–41.
19. Yang S, Jiang M, Li H, Liu Y, Wang L. Assessment of Co-Cr-Ni ternary system by CALPHAD technique. *Rare Met*. 2012 Jan 26; 31(1):75–80.
20. Ansara I, Dinsdale AT, Rand MH. COST 507: Definition of Thermochemical and Thermophysical Properties to Provide a Database for the Development of New Light Alloys—Thermochemical Database for Light Metal Alloys—Volume 2. Luxembourg: Office for Official Publications of the European Communities; 1998.
21. Helander T, Tolochko O. An Experimental Investigation of Possible B2-Ordering in the Al-Cr System. *J Phase Equilibria*. 1999; 20(March 1998):57–60.
22. Dinsdale AT. SGTE data for pure elements. *Calphad*. 1991 Oct; 15(4):317–425.
23. Redlich O, Kister AT. Algebraic Representation of Thermodynamic Properties and the Classification of Solutions. *Ind Eng Chem*. American Chemical Society; 1948 Feb 1; 40(2):345–8.
24. Hillert M, Jarl M. A Model for Alloying Effects in Ferromagnetic Metals. *Calphad*. 1978 Jan; 2(3):227–38.
25. Inden G. The role of magnetism in the calculation of phase diagrams. *Phys B+C*. 1981 Jan; 103(1):82–100.
26. Dupin N, Ansara I. On the sublattice formalism applied to the B2 phase. *Zeitschrift für Met*. 1999; 90:76–85. doi: [10.1107/S0108767309007235](#) PMID: [19349661](#)
27. Sundman B, Ohnuma I, Dupin N, Kattner UR, Fries SG. An assessment of the entire Al-Fe system including D03 ordering. *Acta Mater*. 2009 Jun; 57(10):2896–908.
28. Hillert M. The compound energy formalism. *J Alloys Compd*. 2001 May; 320(2):161–76.
29. Joubert J-M. Crystal chemistry and Calphad modeling of the σ phase. *Prog Mater Sci*. 2008 Mar; 53(3):528–83.
30. Andersson J-O, Helander T, Höglund L, Shi P, Sundman B. Thermo-Calc & DICTRA, computational tools for materials science. *Calphad*. 2002 Jun; 26(2):273–312.

31. Jansson B. Evaluation of parameters in thermochemical models using different types of experimental data simultaneously. Technical Report TRITAMAC-0234. Stockholm, Sweden; 1984.
32. Shang SL, Wang Y, Kim D, Liu Z-K. First-principles thermodynamics from phonon and Debye model: Application to Ni and Ni₃Al. *Comput Mater Sci.* 2010 Feb; 47(4):1040–8.
33. Wang Y, Liu Z-K, Chen L-Q. Thermodynamic properties of Al, Ni, NiAl, and Ni₃Al from first-principles calculations. *Acta Mater.* 2004 May; 52(9):2665–71.
34. Birch F. Finite Elastic Strain of Cubic Crystals. *Phys Rev.* American Physical Society; 1947 Jun 1; 71(11):809–24.
35. Zacherl CL, Shang S-L, Saengdeejing A, Liu Z-K. Phase stability and thermodynamic modeling of the Re-Ti system supplemented by first-principles calculations. *Calphad.* 2012 Sep; 38:71–80.
36. Liu XL, Hargather CZ, Liu Z-K. First-principles aided thermodynamic modeling of the Nb–Re system. *Calphad.* Elsevier; 2013 Jun; 41:119–27.
37. Alers GA. Use of Sound Velocity Measurements in Determining the Debye Temperature of Solids. *Physical Acoustics: Volume 3 Part B.* 1965. p. 1–42.
38. Chen Q, Sundman B. Calculation of Debye Temperature for Crystalline Structures—A Case Study on Ti, Zr, and Hf. *Acta Mater.* 2001; 49:947–61.
39. Lu X-G, Selleby M, Sundman B. Calculations of thermophysical properties of cubic carbides and nitrides using the Debye–Grüneisen model. *Acta Mater.* 2007 Feb; 55(4):1215–26.
40. Shang SL, Wang Y, Liu Z-K. First-principles elastic constants of α - and θ -Al₂O₃. *Appl Phys Lett.* 2007 Mar 7; 90(10):101909.
41. Zunger A, Wei S-H, Ferreira LG, Bernard JE. Special quasirandom structures. *Phys Rev Lett.* 1990 Jul 16; 65(3):353–6. PMID: [10042897](#)
42. Jiang C, Wolverton C, Sofo J, Chen L-Q, Liu Z-K. First-principles study of binary bcc alloys using special quasirandom structures. *Phys Rev B.* 2004 Jun 28; 69(21):214202.
43. Jiang C. First-principles study of ternary bcc alloys using special quasi-random structures. *Acta Mater.* 2009 Sep; 57(16):4716–26.
44. Jiang C, Chen L-Q, Liu Z-K. First-principles study of constitutional point defects in B₂ NiAl using special quasirandom structures. *Acta Mater.* 2005 May; 53(9):2643–52.
45. Lieser AC, Zacherl CL, Saengdeejing A, Liu Z-K, Kecskes LJ. First-principles calculations and thermodynamic re-modeling of the Hf-W system. *Calphad.* 2012 Sep; 38:92–9.
46. Kresse G, Furthmüller J. Efficient iterative schemes for ab initio total-energy calculations using a plane-wave basis set. *Phys Rev B.* 1996 Oct 15; 54(16):11169–86. PMID: [9984901](#)
47. Blöchl PE. Projector augmented-wave method. *Phys Rev B.* 1994 Dec 15; 50(24):17953–79. PMID: [9976227](#)
48. Kresse G, Joubert D. From ultrasoft pseudopotentials to the projector augmented-wave method. *Phys Rev B.* 1999 Jan 15; 59(3):1758–75.
49. Perdew J, Burke K, Ernzerhof M. Generalized Gradient Approximation Made Simple. *Phys Rev Lett.* 1996 Oct 28; 77(18):3865–8. PMID: [10062328](#)
50. Kresse G, Marsman M, Furthmüller J. *VASP: The Guide.* Wein, Austria; 2013.
51. Methfessel M, Paxton AT. High-precision sampling for Brillouin-zone integration in metals. *Phys Rev B.* American Physical Society; 1989 Aug 15; 40(6):3616–21. PMID: [9992329](#)
52. Blöchl PE, Jepsen O, Andersen OK. Improved tetrahedron method for Brillouin-zone integrations. *Phys Rev B.* 1994 Jun 15; 49(23):16223–33. PMID: [10010769](#)
53. Wang Y, Curtarolo S, Jiang C, Arroyave R, Wang T, Ceder G, Chen LQ, Liu ZK. Ab initio lattice stability in comparison with CALPHAD lattice stability. *Calphad.* 2004 Mar; 28(1):79–90.
54. Shang SL, Saengdeejing A, Mei ZG, Kim DE, Zhang H, Ganeshan S, et al. First-principles calculations of pure elements: Equations of state and elastic stiffness constants. *Comput Mater Sci.* 2010 Jun; 48(4):813–26.
55. Dickins GJ, Douglas a. MB, Taylor WH. The crystal structure of the Co–Cr σ phase. *Acta Crystallogr.* 1956 Mar 1; 9(3):297–303.
56. Kittel C. *Introduction to Solid State Physics.* Wiley; 1995.
57. Kamm GN, Alers G a. Low-Temperature Elastic Moduli of Aluminum. *J Appl Phys.* 1964; 35(2):327.
58. Mori N. Magnetic Contribution to the Bulk Modulus of 3d Transition Metals and Alloys. *Phys B.* 1988; 149:226–31.
59. Moruzzi VL, Marcus PM. Antiferromagnetism in 3d Transition Metals. *Phys Rev B.* 1990; 42(13):8361–6. PMID: [9995009](#)

60. Hafner R, Spišák D, Lorenz R, Hafner J. Magnetic ground state of Cr in density-functional theory. *Phys Rev B*. 2002 May; 65(18):184432.
61. Mehl MJ, Osburn JE, Papaconstantopoulos DA, Klein BM. Structural properties of ordered high-melting-temperature intermetallic alloys from first-principles total-energy calculations. *Phys Rev B*. 1990 May; 41(15):10311–23. PMID: [9993438](#)
62. Hammer L, Blum V, Schmidt C, Wieckhorst O, Meier W, Müller S, et al. Role of Co antisite segregation in the CoAl(111) surface. *Phys Rev B*. 2005 Feb; 71(7):075413.
63. Liu XL, VanLeeuwen BK, Shang SS-L, Du Y, Liu Z-K. On the scaling factor in Debye-Grüneisen model: A case study of the Mg-Zn binary system. *Comput Mater Sci*. 2015 Feb; 98:34–41.
64. Stein F, He C, Dupin N. Melting behaviour and homogeneity range of B2 CoAl and updated thermodynamic description of the Al-Co system. *Intermetallics*. 2013 Aug; 39:58–68.
65. Pavl J, Vřešál J, Šob M. Ab initio study of formation energy and magnetism of sigma phase in Cr-Fe and Cr-Co systems. *Intermetallics*. 2010 Feb; 18(2):212–20.
66. Bell HB, Hajra JP, Putland FH, Spencer PJ. The Determination of the Thermodynamic Properties of Cobalt-Chromium Alloys Using Solid-Electrolyte EMF and High-Temperature Calorimetric Techniques. *Met Sci*. 1973 Jan; 7(1):185–90.
67. Downie DB, Arslan F. Enthalpies of formation of (cobalt + chromium) alloys at 473 K. *J Chem Thermodyn*. 1983 Jul; 15(7):645–9.
68. Moskvitina ES, Kuznetsov VN, Guzei LS. Refinement of the Co-Cr-Al Phase-Diagram. *Vestn Mosk Univ Seriya 2 Khimiya (Moscow Univ Chem Bull)*. 1992; 33(4):373–4.